CARBON 50 (2012) 429–435

Available at www.sciencedirect.com

SciVerse ScienceDirect

journal homepage: www.elsevier.com/locate/carbon

Atomic layer etching of graphene for full graphene device fabrication

Woong Sun Lim [a,f], *Yi Yeon Kim* [b], *Hyeongkeun Kim* [a,d], *Sukjae Jang* [a], *Namyong Kwon* [a], *Beyoung Jae Park* [c], *Jong-Hyun Ahn* [a,b], *Ilsub Chung* [a], *Byung Hee Hong* [a,e], *Geun Young Yeom* [a,b,*]

[a] *SKKU Advanced Institute of Nano Technology (SAINT), Sungkyunkwan University, Suwon 440-746, South Korea*
[b] *Department of Advanced Materials Engineering, Sungkyunkwan University, Suwon 440-746, South Korea*
[c] *SEMATECH, 2706 Montopolis Dr., Austin, TX 78741, USA*
[d] *School of Mechanical Engineering, Sungkyunkwan University, Suwon 440-746, South Korea*
[e] *Department of Chemistry, Sungkyunkwan University, Suwon 440-746, South Korea*
[f] *Korea Advanced Nano Fab Center (KANC), Suwon 443-270, South Korea*

ARTICLE INFO

Article history:
Received 16 May 2011
Accepted 29 August 2011
Available online 5 September 2011

ABSTRACT

The possibility of fabricating a full graphene device was investigated by utilizing atomic layer etching (ALET) technology. By using O_2 ALET which functions by oxygen radical adsorption followed by the removal of the oxygen chemisorbed on carbon, the removal of exactly one graphene layer per ALET cycle was detected through the increase of the transmittance by 2.3% after one ALET cycle and by the decrease of the G peak in the Raman spectra. The Raman spectra also showed an increase of the D peak after ALET, indicating the formation of physical damage on the graphene surface layer. This damage was mostly recovered by hydrogen annealing at 1000 °C after ALET. Full graphene field effect transistors (source, drain: 3 layer, channel: 1, 2, 3 layer) were fabricated by reducing the channel layers using ALET, followed by annealing, and the electrical characteristics of the devices showed the possibility of fabricating fully functional graphene devices composed of an all graphene source/drain and graphene channel by utilizing ALET.

1. Introduction

Due to its superior electrical and physical properties, exfoliated graphene has been extensively investigated as the most promising material for future electronic devices [1–4]. Especially, by using chemical vapor deposition (CVD), controlled layers of graphene could be formed on a wafer scale, while keeping the electrical and physical properties similar to those of exfoliated graphene [5–7]. Therefore, these days, electronic devices utilizing a CVD graphene layer as the channel layer are being widely investigated [8–10]. One of the problems encountered in the fabrication of electronic devices using a CVD graphene layer as the channel layer is the contact between the source/drain metal and the channel gate graphene. For example, the contact resistance between the metal source/drain composed of Au(25 nm)/Ti(10 nm) and graphene is as high as 450–800 Ω μm and this can degrade the characteristics of the device [11].

If the source/drain composed of a metal structure is replaced by multi-layer graphene (>3 layers), i.e. if the device can be fabricated with graphene only as a full graphene device, the contact resistance would be greatly reduced and

* *Corresponding author at:* SKKU Advanced Institute of Nano Technology (SAINT), Sungkyunkwan University, Suwon 440-746, South Korea. Fax: +82 31 299 6565.
E-mail address: gyyeom@skku.edu (G.Y. Yeom).
0008-6223/$ - see front matter
doi:10.1016/j.carbon.2011.08.058

the characteristics of the device would be significantly enhanced [11,12]. For the formation of full graphene devices, the use of graphene etching technology to define the source/drain region and the channel region needs to be investigated. For the definition of the device regions, graphene etching has previously been investigated using HeIM (Helium ion beam microscopy) or an O_2 plasma [13,14]. However, these techniques cannot control the etch depth precisely at the atomic layer scale and, therefore, they are not appropriate for the formation of full graphene devices. Especially, the etching of graphene using conventional O_2 plasma can affect the device properties, due to the oxygen remaining at the edges of the graphene layers.

For the formation of full graphene devices, a new graphene layer etching technique which minimizes the physical, chemical, and electrical damage to the device and can control the graphene etch depth at the atomic layer scale needs to be devised. Recently, the layer-by-layer removal of graphene has been reported by selectively depositing Zn on graphene layers followed by treating in a HCl solution [15]. In this study, as a different technique which could be more applicable for smaller device dimension and more reliably, atomic layer etching (ALET) is introduced for the etching of the graphene channel layer and its utilization for the fabrication of a full graphene device and its effect on the device properties were investigated.

2. Experimental

Three layers of graphene transferred onto SiO_2/Si wafers were used as the sample. Monolayer graphene was grown on Cu foil using 460 mTorr pressure CVD at 1000 °C by flowing CH_4/H_2 (28:8 sccm) for ~5 min followed by rapid cooling to room temperature. After the Cu layer was removed in a $FeCl_3$(aq.) solution, the monolayer CVD graphene was transferred onto the SiO_2/Si wafers three times to obtain three layers of graphene on the SiO_2/Si wafers. The details of the CVD graphene fabrication conditions can be found elsewhere [6,7]. The etching of graphene was conducted by neutral beam assisted ALET where the etching source is composed of a three-grid type inductively coupled plasma (ICP) gun and low angle reflector plates. The reflector plates were sloped at 5° to the ion direction in order to neutralize the ions from the ICP gun by the low angle reflection. The graphene ALET process consisted of four steps, viz. adsorption, evacuation, desorption, and evacuation again. During the adsorption step, 20 sccm of O_2 is supplied to the ICP gun, while applying 300 W of 13.56 MHz rf power without applying voltages to the grids of the ICP gun to generate oxygen atoms. During the desorption step, 30 sccm of Ar is supplied to the ICP gun at the same rf power, while applying +30 V to the first grid, −150 V to the second grid, and 0 V to the third grid (located outside of the gun) The first grid voltage controls the energy of the Ar^+ ions, while the second grid controls the flux of the Ar^+ ions. The Ar^+ ions extracted from the ICP gun are neutralized by the low angle reflector plates. The neutralization efficiency was estimated to be higher than 99%. The graphene ALET conditions are described in Table 1. Also, the details of the ALET source can be found elsewhere [19].

Table 1 – O_2 plasma condition of the ICP source during the adsorption step of oxygen radicals and Ar plasma condition of the ICP source during the desorption step of the chemisorbed species.

(a) *O_2 plasma condition*	
Base pressure	3.0×10^{-75} Torr
Working pressure	8.9×10^{-5} Torr
Inductive power	300 W
1st grid voltage	No bias
2st grid voltage	No bias
O_2 gas flow rate	20 sccm
O_2 radical exposure time	5 min
(b) *Ar plasma condition*	
Base pressure	3.0×10^{-7} Torr
Working pressure	4.2×10^{-5} Torr
Inductive power	300 W
1st grid voltage	30 V
2st grid voltage	−150 V
O_2 gas flow rate	30 sccm
Ar neutral beam irradiation time	1 min

The full graphene device was fabricated using the trilayer graphene formed on the SiO_2/Si wafer by defining the device area using a mask layer and by selectively etching the channel graphene layers by ALET. The electrical characteristics of the device were measured by a Keithley 4200 Unit. In addition, the graphene layers etched by ALET were examined by a Micro Raman Spectrometer (Renishaw-Invia Basic) and UV-Spectrometer (Shimadzu UV-3600). The carbon bonding state of the graphene surface was investigated using X-ray Photoelectron Spectroscopy (XPS, Thermo VG, MultiLab 2000, Mg Kα source). Scanning Electron Microscopy (SEM, Hitachi S-4700) was used to observe the number of graphene layers before and after ALET.

3. Results and discussion

Fig. 1 shows the atomic level concept of the graphene ALET process steps. As shown in Fig. 1(a) and (b), (a) during the oxygen adsorption step, the surface of graphene changes from sp^2 bonding to sp^3 bonding due to the chemisorption of oxygen atoms to carbon and (b) the remaining unreacted oxygen is evacuated during the evacuation step.

Fig. 2 shows the Raman spectra of the graphene layers before/after exposure to oxygen molecules or oxygen atoms during the oxygen adsorption step. The graphene surface has a very stable structure and, therefore, if oxygen molecules are used instead of oxygen atoms as shown in Fig. 2(a) and (b), no chemisorption, which would change the graphene bonding from sp^2 to sp^3, is observed even after the exposure of the surface to oxygen molecules for 10 min, while chemisorption is observed after its exposure to oxygen atoms for 1 min due to their high reactivity as shown in Fig. 2(a) and (c). Fig. 3 shows (a) the XPS C1s peak of the graphene surface deconvoluted into sp^2 C–C binding (284.6 eV), sp^3 C–C binding (285.7 eV), and C–O binding (288.0 eV) and (b) the atomic percentages of C–O bonding, sp^3 C–C bonding, and sp^2 C–C bonding of the graphene surface measured after the various steps of the etch cycle. As shown in this figure, before the etching

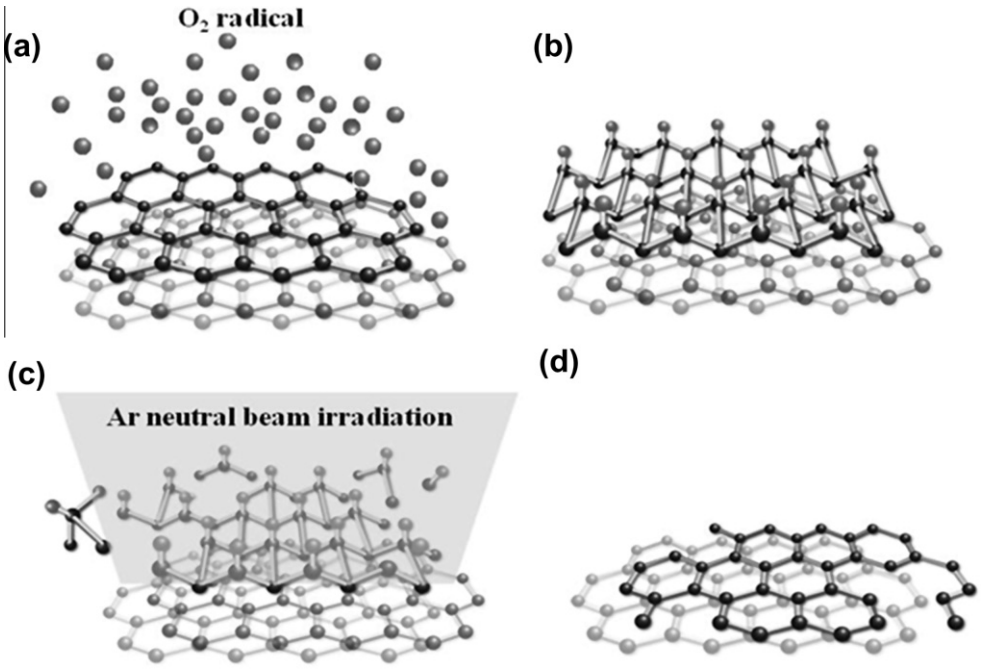

Fig. 1 – Concept of O_2 ALET for graphene. The graphene ALET process is composed of four steps. (a) The oxygen adsorption step, in which the surface of graphene changes from sp^2 bonding to sp^3 bonding by the chemisorption of oxygen atoms to carbon. (b) The evacuation step, in which the remaining unreacted oxygen is evacuated. (c) The desorption of chemisorbed species, in which the chemisorbed C–O with sp^3 bonding is desorbed from the oxygen chemisorbed graphene surface by the irradiation of the 30 eV Ar particle beam, while the carbon with sp^2 bonding under the C–O bonding remains unetched due to the high binding energy. (d) The evacuation step, in which the etch byproducts and desorption gas are removed.

process, the graphene surface consists mostly of sp^2 bonding (>73 %) with some sp^3 bonding. However, after its exposure to oxygen atoms, due to the chemisorption of oxygen, C–O bonding (19.17 %) is formed while the amount of sp^3 bonding (23.49 %) is not changed significantly with the corresponding decrease of the sp^2 bonding [16]. As the Ar particle beam with an energy of 30 eV is irradiated, as shown in Fig. 1(c), only the chemisorbed C–O with sp^3 bonding is desorbed from the oxygen chemisorbed graphene surface, while carbon with sp^2 bonding under the C–O bonding remains unetched, due to the high binding energy of sp^2 bonding and the low bonding energy between the graphene layers. After the desorption step, the chamber is evacuated again to remove the etch byproducts and the desorption gas remaining in the chamber. After the completion of the four etch steps (that is, after one cycle of ALET), one monolayer of graphene is completely removed if oxygen atoms are chemisorbed onto the entire surface of graphene (during the oxygen adsorption step) and all of the resulting chemisorbed CO is removed from the graphene layer surface (during the desorption step). The complete removal of CO bonding on the graphene surface after one cycle of ALET was observed by XPS, as shown in Fig. 3(a) and (b) (after one cycle of ALET). The bilayer of CVD graphene etched by ALET was observed by UV, Raman, and SEM spectroscopy and the results are shown in Fig. 4(a–d). A previous study showed a decrease of the optical transmittance of about 2.3% per monolayer of graphene [7].

As shown in Fig. 4(a), the optical transmittance of the bilayer of graphene measured at 550 nm was 94.7 %, and after each cycle of ALET the optical transmittance was increased by about 2.3–2.4%, indicating the removal of the monolayer of graphene by ALET. Fig. 4(b) shows the Raman spectra measured before and after the ALET of the bilayer of CVD graphene. The exfoliated graphene shows a ratio of G/2D of about 1.0, however the graphene layer grown by CVD and stacked by the transfer of monolayers of graphene shows Raman characteristics similar to those of monolayer graphene (G/2D > 1), due to the lack of an AB stacking sequence [7]. As shown in the figure, after two cycles of ALET, the G and 2D peaks completely disappeared, indicating the complete removal of the bilayer of graphene. The removal of one layer of the bilayer of CVD graphene by one cycle of ALET was also observed by SEM after the partial etching of the graphene sheet composed of bilayer/monolayer graphene, as shown inside of the rectangular pattern of Fig. 4(c). The graphene sheet was selectively etched by ALET after patterning by photoresist. The photoresist was removed after the etching process. As shown in Fig. 4(d), after one cycle of ALET, throughout the substrate, only the unmasked bilayer graphene area changed to monolayer graphene, while the unmasked monolayer graphene area changed to zero layer graphene. The shape of the bilayer graphene also remained unchanged, indicating that there was no undercutting of the graphene layer during ALET. Therefore, it is believed that ALET can be utilized to achieve the etching of graphene layers precisely, anisotropically, and uniformly over a large area substrate (all of the wafer area showed the same etching of one graphene layer per cycle of ALET), which is required for the fabrication of graphene nanodevices.

Even though ALET can control the etching on the atomic layer scale, the graphene surface appeared to be partially

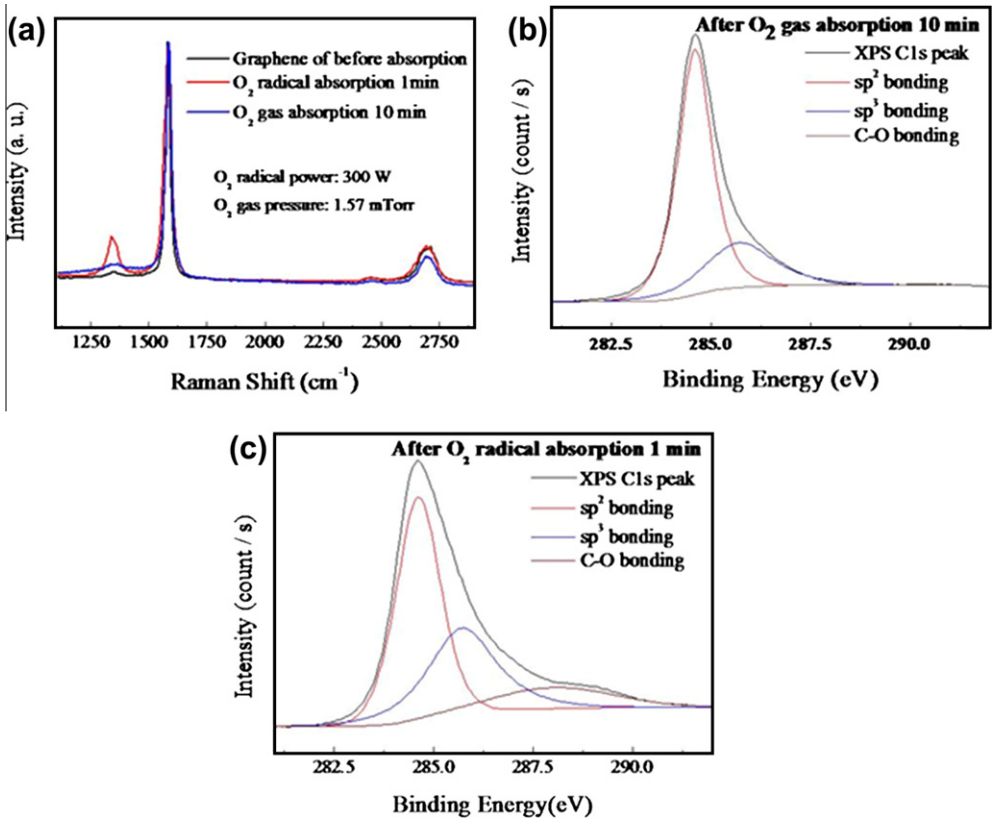

Fig. 2 – (a) Raman spectra of graphene layer before/after exposure to oxygen molecules/radicals. The exposure of the graphene layer to the oxygen molecules for 10 min did not change the Raman spectra. However, its exposure to oxygen radicals for 1 min led to the appearance of the D peak, which indicates the adsorption of oxygen to graphene. (b and c) show the XPS peak (C1s) of the graphene surface measured after its exposure to oxygen molecules for 10 min (b) and after its exposure to oxygen radicals for 1 min (c). As shown in these figures, no CO bonding is observed after the exposure to oxygen molecules. However, after exposure to oxygen radical, an increase in the amount of CO bonding and sp^3 bonding with a corresponding decrease of sp^2 bonding is observed.

damaged after the etching process. Damage was observed due to the higher sp^3 bonding (36.49%) after one cycle of ALET compared to that of the as-received graphene (24.01%), as shown in Fig. 3, and also by the formation of the D peak and the decrease of the 2D peak after the ALET, as shown in Fig. 4(b). When the energy distribution of the Ar^+ ion beam extracted by the Ar ICP ion gun was investigated, the Ar ion showed an additional high energy peak ~48 eV in addition to 30 eV peak required for the desorption of C–O bonding during the ALET. The increase of sp^3 bonding after the ALET

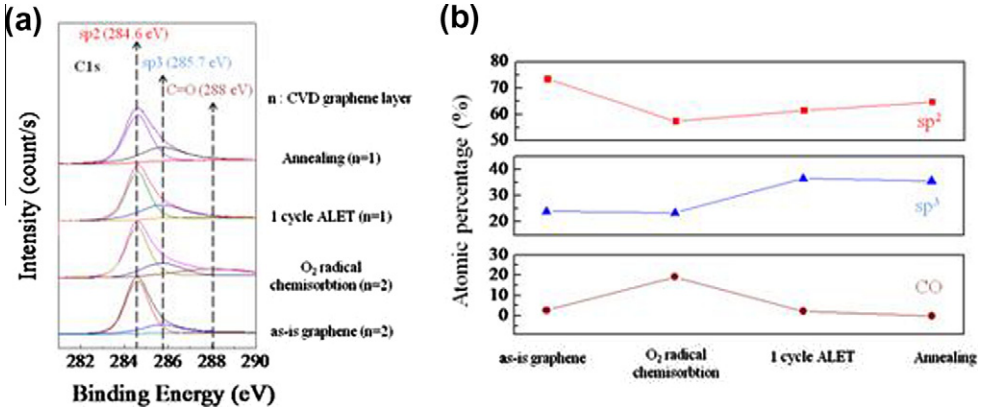

Fig. 3 – (a) XPS peak (C1s) of the graphene surface measured after each ALET process step (as-is, O_2 radical chemisorption, 1 cycle ALET, annealing). (b) Atomic percent of surface bonding measured using XPS after the ALET process steps (as-is, O_2 radical chemisorption, 1 cycle ALET, annealing).

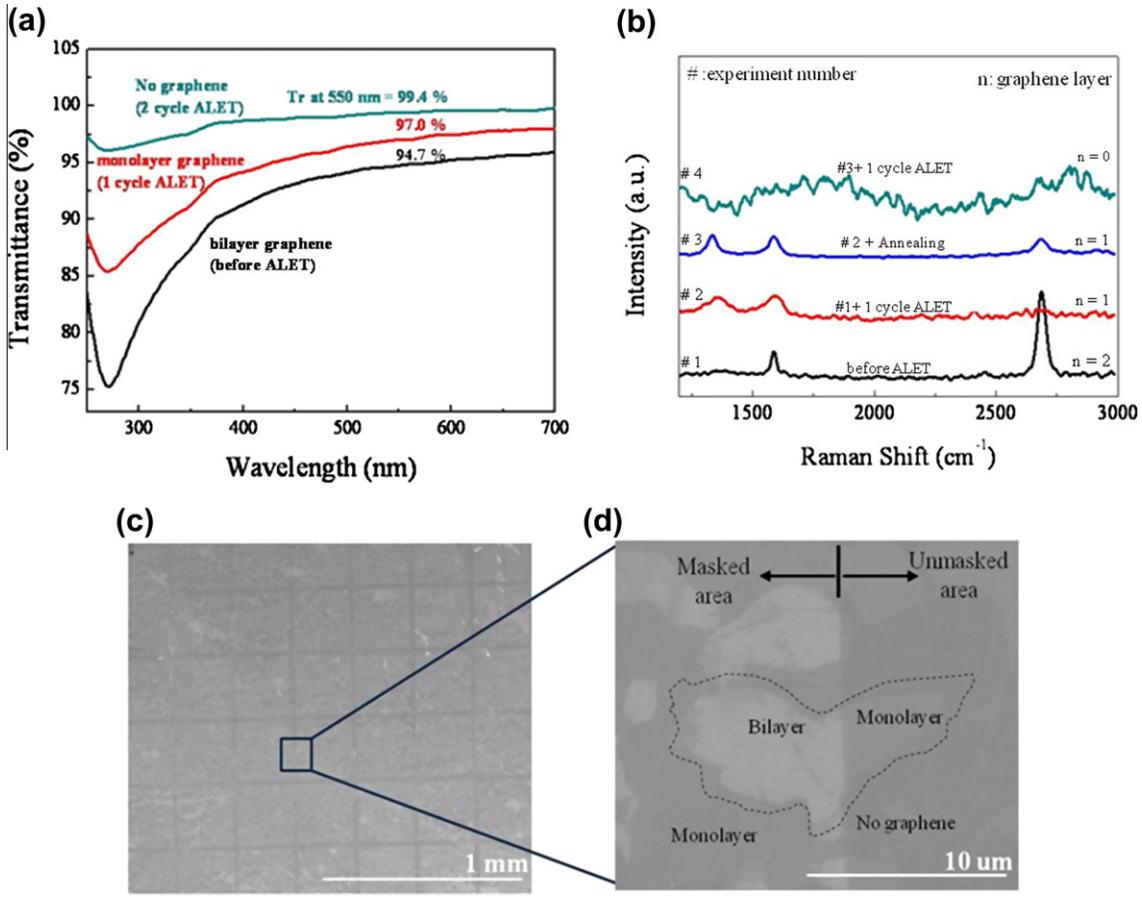

Fig. 4 – (a) Optical transmittance of bilayer graphene before and after ALET cycles. The black line is the transmittance of the bilayer graphene (before ALET). Other transmittance spectra were obtained after the ALET cycles (red line: after 1 cycle of ALET, green line: after 2 cycles of ALET). After each ALET cycle, the optical transmittance measured at 550 nm is increased by about 2.3%. (b) Raman spectra of bilayer graphene measured after each ALET cycle and after the annealing of the 1 cycle etched graphene. (c and d) SEM images of a patterned graphene sheet (bilayer graphene mixed with monolayer graphene) which has been etched by 1 cycle of ALET. The square-shaped masked area in (c) shows the remaining bilayer/monolayer graphene, while the open edge area shows the monolayer/no graphene, indicating the etching of one graphene layer by 1 cycle of ALET. All of the exposed substrate area showed the uniform removal of a monolayer of graphene after 1 cycle of ALET and the graphene layer was etched without undercutting. (For interpretation of the references to color in this figure legend, the reader is referred to the web version of this article.)

is believed to be related to the physical bombardment by the high energy beam (~48 eV) extracted from the plasma gun during the desorption step, in addition to the beam energy (30 eV) required for ALET, and this problem needs to be resolved in the near future. The physically damaged graphene surface was mostly recovered by annealing in a 130 mTorr H_2/He environment at 1000 °C for 30 min, as observed in Fig. 3, due to the decrease of the sp^3 bonding and the increase of the sp^2 bonding after annealing to levels close to those of the graphene surface before etching. The Raman spectra in Fig. 4(b) also showed the recovery of the 2D peak formed by ALET after annealing, indicating the recrystallizaton of the damaged graphene layer. However, the D peak still remained even after the annealing process, indicating the incomplete recovery, possibly due to the insufficient amount of carbon on the graphene surface for complete recrystallization [17], because an annealing process at a higher annealing temperature did not show significant improvement in the recovery.

Using the ALET process followed by annealing, full metal–oxide-semiconductor (MOS) devices composed of a graphene source, graphene drain, and graphene channel were fabricated. The fabrication sequence is schematically shown in Fig. 5(a). The trilayer graphene transferred to a (200 nm) SiO_2/n + Si wafer was patterned to define the device region composed of a source, drain, and gate channel using a 20 nm thick Au etch mask and by using a conventional oxygen ICP plasma. The channel graphene layer was etched by ALET after masking the source/drain region by an Au mask to control the number of channel graphene layers. The inset picture in Fig. 5(b) shows an optical image of the fabricated full graphene device composed of a monolayer graphene channel and a trilayer source/drain. The electrical characteristics of the full graphene devices with different graphene

channel layers obtained by ALET were observed and the results are shown in Fig. 5(b–d). As shown in Fig. 5(b), the V_D–I_D (width: 2 μm, length: 10 μm) was linear and, after each cycle of ALET, I_D was decreased, indicating the increase of the resistance of the channel caused by the decrease in the number of channel graphene layers [18]. The characteristics of V_{GS}–I_D (width: 10 μm, length: 10 μm) were measured for the channels with the trilayer graphene and monolayer graphene (after 2 cycles of ALET) and the results are shown in Fig. 5(c). As shown in the figure, similar to the trilayer graphene channel, the annealed monolayer graphene channel showed the general characteristics of graphene. In addition, the characteristics of V_D–I_D (width: 2 μm, length: 10 μm) measured as a function of V_{GS} also showed that the annealed graphene channel layer exhibits the general characteristics of graphene, indicating the possibility of fabricating full graphene MOS devices using ALET technology. However, the electrical characteristics of the fabricated graphene transistors were generally poor and it is not only related to the partial damage to graphene during the ALET but also to the quality of the CVD graphene and to the AB stacking misfit of the stacked CVD graphene multilayer used in the experiment. Therefore, it is believed that, the improved MOS device characteristics can be obtained by removing the high energy peak (~48 eV) during the desorption step of the ALET and by using the high quality multilayer graphene without AB stacking misfit.

4. Conclusion

In summary, we demonstrated the precise etching of a monolayer of graphene per etch cycle uniformly over a large area using O_2 ALET. After ALET, damage to the graphene layer was observed related to the high energy Ar bombardment from the ICP source, but this damage could be mostly recovered by annealing in an H_2/He environment. Full graphene devices composed of a graphene source/drain and graphene channel were fabricated by etching the channel graphene layer using ALET followed by annealing. The fabricated devices did not show perfect graphene device characteristics, possibly due to the AB stacking misfits, due to the transfer of the CVD graphene layers, in addition to the damage remaining on the graphene channel layer. However, the possibility of fabricating full graphene devices composed of only graphene on the substrate in the near future was demonstrated by utilizing ALET technology.

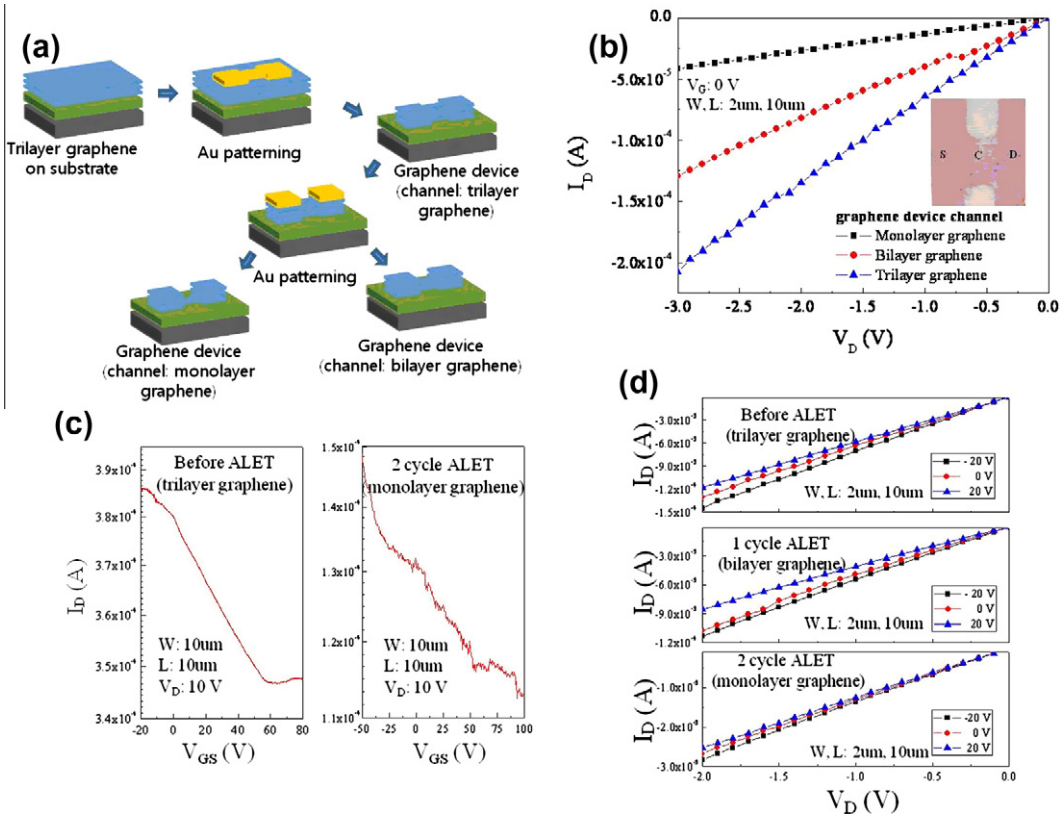

Fig. 5 – (a) Fabrication sequence of a full graphene device composed of a graphene source, graphene drain, and graphene channel. (b) Drain current (I_D) versus drain–source voltage (V_D), recorded for different graphene device channel layers (device channel width 2 μm and length 10 μm). The inset figure is the SEM image of a fabricated full graphene device with trilayer source/drain and monolayer graphene channel. (c) Transfer characteristics at V_D = 10 V for full graphene devices with different graphene channel layers (trilayer and monolayer channel; device channel width 10 μm and length 10 μm). (d) Drain current (I_D) versus drain–source voltage (V_D), recorded at different gate voltages for full graphene devices with different graphene channel layers (device channel width 2 μm and length 10 μm).

Acknowledgment

This work supported by a grant from the National Research Foundation of Korea funded by the Korean Government (MEST) (2010-0026248).

REFERENCES

[1] Geim AK, Novoselov KS. The rise of graphene. Nat Mater 2007;6:183–91.
[2] Elias DC, Nair RR, Mohiuddin TMG, Morozov SV, Blake P, Halsall MP, et al. Control of graphene's properties by reversible hydrogenation: evidence for graphene. Science 2009;323:610–3.
[3] Lee C, Wei XD, Kysar JW, Hone J. Measurement of the elastic properties and intrinsic strength of monolayer graphene. Science 2008;321:385–8.
[4] Bunch JS, Verbridge SS, Alden JS, Van der Zande AM, Parpia JM, Craighead HG, et al. Impermeable atomic membranes from graphene sheets. Nano Lett 2008;8:2458–62.
[5] Kim KS, Zhao Y, Jang H, Lee SY, Kim JM, Kim KS, et al. Large-scale pattern growth of graphene films for stretchable transparent electrodes. Nature 2009;457:706–10.
[6] Lee YB, Bae SK, Jang H, Jang SJ, Zhu SE, Sim SH, et al. Wafer-scale synthesis and transfer of graphene films. Nano Lett 2010;10:490–3.
[7] Bae SB, Kim HK, Lee YB, Xu XF, Park JS, Zheng Y, et al. Roll-to-roll production of 30-inch graphene films for transparent electrodes. Nat Nanotech 2010;5:574–8.
[8] The international technology roadmap for semiconductors. http://www.itrs.net/Links/2009ITRS/Home2009.htm [Semiconductor Industry Association, 2009].
[9] Frank S. Graphene transistors. Nat Nanotech 2010;5:487–96.
[10] Lin Y-M, Dimitrakopoulos C, Jenkins KA, Farmer DB, Chiu H-Y, Grill A, et al. 100-GHz transistors from wafer-scale epitaxial graphene. Science 2010;327:662.
[11] Russo S, Cracuin MF, Yamamoto Y, Morpurgo AF, Tarucha S. Contact resistance in graphene-based devices. Physica E 2010;42:677–9.
[12] Venugopal A, Colombo L, Vogel EM. Contact resistance in few and multilayer graphene devices. Appl Phys Lett 2010;96:013512-1–3.
[13] Lemme MC, Bell DC, Williams JR, Stern LA, Baugher BWH, Jarillo-Herrero P, et al. Etching of graphene devices with a helium ion beam. ACS Nano 2009;3:2674–6.
[14] Fredriksson H, Chakarov D, Kasemo B. Patterning of highly oriented pyrolytic graphite and glassy carbon surfaces by nanolithography and oxygen plasma etching. Carbon 2009;47:1335–42.
[15] Dimiev A, Kosynkin V, Sinitskii A, Slesarev A, Sun Z, Tour JM. Layer-by-layer removal of graphene for device patterning. Science 2011;331:1168–72.
[16] Park SP, An JH, Piner RD, Jung I, Yang DX, Velamakanni A, et al. Aqueous suspension and characterization of chemically modified graphene sheets. Chem Mater 2008;20:6592–4.
[17] Krauss B, Lohmann T, Chae DH, Haluska M, von Klitzing K, Smet JH. Laser-induced disassembly of a graphene single crystal into a nanocrystalline network. Phys Rev B 2009;79:165428–9.
[18] Sui Y, Appenzeller J. Screening and interlayer coupling in multilayer graphene field-effect transistors. Nano Lett 2009;9:2973–7.
[19] Lee DH, Bae JW, Park SD, Yeom GY. Development of a low angle forward neutral oxygen beam for materials processing. Thin Solid Films 2001;398:647–51.